SUPPLEMENTAL MATERIAL

Collagen turnover in relation to risk factors and hemodynamics in human intracranial aneurysms

Katharina A.M. Hackenberg[1] MD, Hamidreza Rajabzadeh-Oghaz[2] MS, Rita Dreier[3] PhD, Bruce A. Buchholz[4] PhD, Ali Navid[5] PhD, David M. Rocke[6] PhD, Amr Abdulazim[1] MD, Daniel Hänggi[1] MD, Adnan Siddiqui[7] MD, PhD, R. Loch Macdonald[8] MD, PhD, Hui Meng[9] PhD, Nima Etminan[1] MD

[1]*Department of Neurosurgery, University Hospital Mannheim, Medical Faculty Mannheim, University of Heidelberg, Mannheim, Germany*
[2]*Canon Stroke and Vascular Research Center, Department of Mechanical and Aerospace Engineering, University at Buffalo, Buffalo, New York, USA*
[3]*Institute for Physiological Chemistry and Pathobiochemistry, Westfalian Wilhelms-University, Münster, Germany*
[4]*Center for Accelerator Mass Spectrometry, Lawrence Livermore National Laboratory, Livermore, CA, USA*
[5]*Biosciences and Biotechnology Division, Lawrence Livermore National Laboratory, Livermore, CA, USA*
[6]*Division of Biostatistics, University of California, Department of Public Health Sciences (Medicine), Davis, California, USA*
[7]*Canon Stroke and Vascular Research Center, Department of Neurosurgery, Jacobs School of Medicine and Biomedical Sciences, Department of Radiology, Jacobs School of Medicine and Biomedical Sciences, Department of Neurosurgery, Gates Vascular Institute, Kaleida Health, Jacobs Institute, University at Buffalo, Buffalo, New York, USA*
[8]*Department of Neurological Surgery, UCSF Fresno, Fresno, California, USA; Department of Surgery, University of Toronto, Toronto, Ontario, Canada*
[9]*Canon Stroke and Vascular Research Center, Department of Mechanical and Aerospace Engineering, Department of Biomedical Engineering, Department of Neurosurgery, Jacobs School of Medicine and Biomedical Sciences, University at Buffalo, Buffalo, New York, USA*

Corresponding author:
Nima Etminan MD
Department of Neurosurgery, University Hospital Mannheim, University of Heidelberg, Theodor-Kutzer-Ufer 1-3, 68167 Mannheim, Germany
Phone: +49 621 383 2360, Fax: +49 621 383 2004
nima.etminan@umm.de

Key words: intracranial aneurysms, birth dating, collagen turnover, wall shear stress

Supplemental Methods

We previously described tissue processing, collagen purification and the corresponding ^{14}C birth dating method in IA samples derived from patients undergoing surgical repair for IA [1]. The ^{14}C birth dating analysis, the mathematical model of collagen turnover and CFD simulations were performed independent from and blinded to each other.

Mathematical model of collagen turnover

The mathematical model for calculating turnover rates of collagen is based on previous models of tissue regeneration and collagen turnover [2-4]. For calculations of collagen turnover rates, the following assumptions were made:

1. Constant degradation rate (γ, unit year^{-1}): all collagens, regardless of their age, degradation at the same rate.
2. γ does not vary with the age of the sample donor.
3. Collagens are produced at a constant rate, invariant with age of the sample donor.
4. The amount of collagen in individuals is at homeostasis, i.e., each degraded collagen is replaced and the overall number of collagens in the systems does not change

The age of collagen (a, years) can be calculated using:

$$a = t - t_0 \qquad (1)$$

t_0 is the time of production of collagen; a [months] = a*12, a [days] = a*365.

The equation describing the time course of change in number of collagens of age a, n_a would be:

$$\frac{dn_a}{dt} = -\gamma n_a + \delta_{t-t_0}(a)N_0 \qquad (2)$$

N_0 is the total number of collagens at the beginning of simulation. In case of our calculations the beginning of the simulation is time of birth of the sample donor.

δ_{t-to} is the Dirac delta function to ensure that collagens of age a are only formed at the time of their production. The total number of collagens ($N(t)$) in an individual of age t can be calculated using the formula:

$$N(t) = \sum_{a=0}^{A} n_a \qquad (3)$$

A is the number different n_a that we track during our simulations. It is worth noting that given our assumption of homeostasis, $N(t)=N_0$ at all times. For our calculations of collagen turnover, we solved equation (2) using Euler's method with a time step of 0.019 year (~2 weeks).

The variable in our simulations is the value of degradation rate γ. When calculating turnover rates in either individuals or populations we began by generating a continuous ^{14}C bomb-curve by linearly extrapolating between growing season averages of experimental measurements. This needed to be done only one time. Next, in an iterative fashion we:

1. Chose a γ value
2. Solved for the number of collagens of age a during the entire period from a person's birth date until the day when the collagen sample was collected.
3. We calculated the fraction of total collagens that had a certain age

$$F_a = \frac{n_a}{N_0}$$

4. We then calculated the expected ^{14}C level for the chosen γ value in the collected sample $X(t,\gamma)$

$$X(t,\gamma) = \sum_{a=0}^{A} F_a \, {}^{14}C(t_0)$$

Where $^{14}C(t_0)$ is the value of ^{14}C in the atmosphere on the day collagens of age a were formed.

5. Calculated the value *SSE*, the sum of square of error between $X(t,\gamma)$ and measured ^{14}C values.
6. Repeated the process starting from step 1 with a new slightly higher or lower (±0.5 %) γ value, depending on which direction lowered the value of *SSE* until the changes in γ would not lower *SSE*.
7. For population simulations (e.g. smokers), the same process was used except the goal was to reduce SSE for the all the samples from that population.

Image and image segmentation

To study the relation of collagen turnover rates and hemodynamics computed by CFD in human IA, 3D computed tomography angiographic (CTA) data were collected. The 3D CTA images of all patients were segmented using open-source Vascular Modeling Toolkit (VMTK, http://www.vmtk.org) [5]. VMTK is a semiautomated tool that uses a level-set method to place a contour at regions with maximum gradient intensity. After segmentation, a surface mesh for IA with surrounding parent vessels was generated using the threshold-based marching cubes algorithm [5]. Exclusion criteria were CTA data with a low image quality with a voxel size > 0.5 mm or movement artifacts and a location of IA at the base level of the skull, which makes the segmentation difficult due to the presence of bone.

Computational fluid dynamics

The inlet and outlet surfaces of IA geometries were extended by 10 times of parent artery diameters to ensure fully developed flow at the inlet and avoid backflow at the outlets. We used commercial software STAR-CCM+ (Siemens PLM, Plano, TX, USA) for volumetric mesh generation and CFD simulations. IA geometries were discretized using volumetric polyhedral elements with a base size of 0.15 mm and four refined prism layers (thickness of 0.015 mm) to provide fine mesh resolution on lumen. Meshing resulted in ~1-4 million volumetric elements to represent the discretized flow domains in all the cases. A time step of 0.001 s was used for temporal resolution. The flow-governing Navier-Stokes equations were discretized using second-order upwind and first-order schemes for spatial and temporal discretization, respectively. For all the simulations, the wall was assumed to be rigid, and blood was considered as a Newtonian fluid with a viscosity of μ=3.5 cP and a density of ρ=1056 kg/m3. The residuals for convergence criteria for mass and momentum equations were set as 10-5. The patient-specific arterial flow was not available in our study. Therefore, we used a normalized velocity waveform derived from transcranial Doppler ultrasound measurements in the internal carotid artery of a healthy subject (32-year-old man) [6]. The waveform was scaled by literature-derived flow rates for the given vessel location (internal carotid artery: 4.6 ml/s, middle cerebral artery: 2 ml/s). For outlets, the flow rate was prescribed to be proportional to the vessel diameter cubed, based on Murray's Law of principle of optimum work [7]. CFD simulations were conducted for three cardiac cycles and the third one was used for post-processing.

Using the obtained flow field in each IA, we calculated the luminal wall shear stress (WSS). WSS is the tangential frictional stress caused by the action of flowing blood on the vessel wall endothelium [8]. We calculated aneurysm-averaged values for the following parameters (see table I: Time-averaged WSS, which is spatiotemporal WSS magnitude average through the cardiac cycle; normalized WSS (NWSS), which is WSS further normalized by the spatiotemporal average wall shear stress of the parent vessel; oscillatory shear index (OSI), which measures the directional change of the WSS through the cardiac cycle; relative residence time (RRT), which quantifies the stasis of blood near the aneurysm wall.

Risk factors

Risk factors for IA instability, such as arterial hypertension, current smoking, IA irregularity, IA size and IA site were assessed regarding a possible association with IA hemodynamics and

collagen turnover. Arterial hypertension was defined as systolic blood pressure > 140 mmHg or diastolic blood pressure > 90 mmHg on admission or previous diagnosis of hypertension or antihypertensive treatment. Current smoking was defined as a risk factor, if the patients had smoked ≥ 100 cigarettes in their lifetime and smoked cigarettes regularly [9]. Irregularity was defined as multiple lobes, presence of daughter-sac or blebs. IA size was measured in Millimeter (mm).

Histological stainings

For visualization of collagen in IA samples Movat Pentachrome (Movat Pentachrome Stain Kit, Abcam, Cambrigde, United Kingdom) and Picrosirius Red (Picro Sirius Red Stain Kit, Abcam, Cambrigde, United Kingdom) stainings were performed on 8 µm longitudinal cryosections through IA dome and IA transition zone (zone between dome and neck). For microscopy Leica DMIRB Inverted Leica Modulation Contrast Microscope (Leica Microsystems GmbH, Wetzlar, Germany) was used with image analysis software Leica Application Suite Version 4.4 (Leica Microsystems GmbH, Wetzlar, Germany. To assess maturity of collagen linear-polarized microscopy was performed in cryosections stained with Picrosirius Red: immature collagen illustrates predominantly yellow-green birefringence, mature collagen shows predominantly orange-red birefringence [10, 11].

Statistical analyses

For statistical analyses the SPSS statistics software package 25 (IBM Corporation, Armonk, New York, USA) was used. If not indicated otherwise, data are reported as means (M) ± standard deviation (SD). The Mann-Whitney test was used for comparison of two independent conditions for non-normally distributed data as well as for normally distributed data due to small sample sizes. In case of an individual infinite collagen turnover rate, individual collagen turnover rates were at least ≥ 2000 % per year, whereas several values were distinctly higher; such turnover rates were conservatively defined as 2000 % per year for further statistical analyses. To identify CFD parameters indicative of collagen turnover in IA, morphologic and hemodynamic parameters were correlated with collagen turnover rates using Pearson correlation for continuous variables and Spearman correlation for non-normally distributed data. Receiver operating characteristic (ROC) analysis was performed to define thresholds for rapid versus slow collagen turnover for each parameter, the cut-off value for differentiation was 1200 % per year. To identify predictors for rapid collagen turnover binary logistic regression analyses were performed with the same cut-off value for differentiation of collagen turnover, the likelihood ratio statistic was performed as a priori test. The value for statistically significant differences was set at probability (p) value < 0.05.

Supplemental Tables

Parameter	Definition
Wall shear stress	$\frac{1}{T}\int_0^T \lvert wss_i \rvert dt$ Normalized by spatial average of parent vessel WSS
Maximum wall shear stress	$maximum_{sac}(\frac{1}{T}\int_0^T \lvert wss_i \rvert dt)$ Normalized by spatial average of parent vessel WSS
Oscillatory shear index	$\frac{1}{2}\left\{1 - \frac{\lvert \int_0^T wss_i\, dt \rvert}{\int_0^T \lvert wss_i \rvert dt}\right\}$
Relative residence time	$\frac{1}{(1 - 2 \times \mathrm{OSI}) \times \mathrm{WSS}}$

Table I: Mathematical definitions of the hemodynamic parameters: These hemodynamic parameters are spatial distributions. For each IA, we reported the spatially averaged values of the aneurysm sac.
Abbreviations: IA indicates Intracranial aneurysm; OSI, Oscillatory shear index; t, Time; T, cardiac cycle; WSS, Wall shear stress; WSS_i, Instantaneous wall shear stress.

		^{14}C birth dating cohort	**CFD cohort**
Intracranial aneurysms		46	20
Patients		43	20
Sex	Female	29 (63.0)	15 (75.0)
	Male	17 (37.0)	5 (25.0)
Age ± SD [years]		55.1 ± 11.5	54.6 ± 9.7
Rupture status	Yes	36 (78.3)	14 (70.0)
	No	10 (21.7)	6 (30.0)
Aneurysm irregularity	Yes	27 (58.7)	9 (45.0)
	No	19 (41.3)	11 (55.0)
Arterial hypertension	Yes	23 (50.0)	8 (40.0)
	No	23 (50.0)	12 (60.0)
Smoking	Yes	16 (34.8)	9 (45.0)
	No	30 (65.2)	11 (55.0)
Arterial hypertension and/or smoking	Yes	34 (73.9)	15 (75.0)
	No	12 (26.1)	5 (25.0)
Diameter± SD [mm]		8.67 ± 5.59	7.55 ± 2.21
Aneurysm location	ICA with PCOM	10 (21.7)	6 (30.0)
	ICA without PCOM	1 (2.2)	1 (5.0)
	PCOM	9 (19.6)	5 (25.0)
	MCA	21 (45.7)	9 (45.0)
	ACA, ACOM	7 (15.2)	5 (25.0)
	Posterior	8 (17.4)	0 (0.0)

Table II: Characteristics of the ^{14}C birth dating cohort (calculation of collagen turnover rates) and computational fluid dynamics cohort.
Numbers are given in n (%) or Mean ± SD.
Abbreviations: ACA indicates Anterior cerebral artery; ACOM, Anterior communicating artery; CFD, Computational fluid dynamics; ICA, Internal carotid artery; MCA, Middle cerebral artery; PCOM, Posterior communicating artery; SD, Standard deviation

Sample No.	Sex	Patient age	Rupture status	Fraction modern (± SD)	Predicted fraction modern (± % error)									
					All	Female	Male	Ruptured	Un-ruptured	Modifiable risk factor (AHT and/or smoking)	No modifiable risk factor	AHT	Smoking	Irregularity
1	Female	56	Yes	1.068 (± 0.005)	1.056 (± 1.2)	1.056 (± 1.1)		1.055 (± 1.2)			1.063 (± 0.3)			1.055 (± 1.2)
2	Male	77	Yes	1.057 (± 0.004)	1.055 (± 0.2)		1.054 (± 0.3)	1.058 (± 0.2)		1.053 (± 0.4)		1.053 (± 0.4)		
3	Male	77	Yes	1.052 (± 0.004)	1.055 (± 0.3)		1.054 (± 0.3)	1.058 (± 0.3)		1.053 (± 0.2)		1.053 (± 0.1)		
4	Female	53	Yes	1.035 (± 0.004)	1.054 (± 1.8)	1.054 (± 1.8)		1.053 (± 1.8)			1.062 (± 2.7)			1.053 (± 1.8)
5	Female	74	No	1.053 (± 0.004)	1.054 (± 0.0)	1.054 (± 0.0)			1.054 (± 0.0)	1.051 (± 0.3)		1.051 (± 0.3)		
6	Male	57	Yes	1.043 (± 0.004)	1.053 (± 0.9)		1.052 (± 0.9)	1.053 (± 1.0)		1.050 (± 0.6)		1.049 (± 0.6)		
7	Female	47	Yes	1.062 (± 0.009)	1.052 (± 0.9)	1.053 (± 0.9)		1.052 (± 0.9)			1.061 (± 0.1)			
8	Female	47	Yes	1.109 (± 0.011)	1.052 (± 5.1)	1.053 (± 5.1)		1.052 (± 5.1)			1.061 (± 4.3)			
9	Female	61	Yes	1.067 (± 0.010)	1.052 (± 1.4)	1.052 (± 1.3)		1.052 (± 1.4)		1.049 (± 0.7)		1.048 (± 1.7)		
10	Male	48	No	1.050 (± 0.007)	1.052 (± 0.1)		1.051 (± 0.0)		1.052 (± 0.1)	1.048 (± 0.2)		1.048 (± 0.3)	1.050 (± 0.0)	
11	Female	74	No	1.036 (± 0.004)	1.050 (± 1.3)	1.050 (± 1.4)			1.050 (± 1.4)		1.059 (± 2.2)			
12	Female	49	Yes	1.064 (± 0.012)	1.050 (± 1.3)	1.050 (± 1.3)		1.050 (± 1.3)		1.047 (± 0.6)			1.048 (± 1.4)	1.050 (± 1.3)
13	Female	53	Yes	1.037 (± 0.004)	1.049 (± 1.2)	1.050 (± 1.2)		1.049 (± 1.2)		1.047 (± 1.0)			1.048 (± 1.1)	1.049 (± 1.2)
14	Male	51	Yes	1.057 (± 0.008)	1.049 (± 0.7)		1.049 (± 0.8)	1.049 (± 0.7)		1.047 (± 1.0)		1.047 (± 1.0)		1.049 (± 0.8)
15	Female	43	Yes	1.037 (± 0.005)	1.049 (± 1.1)	1.049 (± 1.2)		1.048 (± 1.1)		1.047 (± 1.0)		1.047 (± 1.0)		

16	Male	52	Yes	1.051 (± 0.005)	1.048 (± 0.3)		1.048 (± 0.4)	1.048 (± 0.3)		1.047 (± 0.5)			1.047 (± 0.4)	1.048 (± 0.3)
17	Male	54	Yes	1.039 (± 0.004)	1.048 (± 0.8)		1.047 (± 0.8)	1.048 (± 0.8)		1.046 (± 0.6)		1.046 (± 0.6)		1.048 (± 0.8)
18	Female	62	Yes	1.043 (± 0.004)	1.048 (± 0.5)	1.048 (± 0.5)		1.048 (± 0.5)		1.046 (± 0.3)			1.047 (± 0.3)	
19	Female	48	No	1.053 (± 0.005)	1.048 (± 0.5)	1.048 (± 0.5)			1.043 (± 0.5)		1.056 (± 0.3)			
20	Female	62	No	1.038 (± 0.004)	1.047 (± 0.9)	1.048 (± 0.9)			1.048 (± 1.0)	1.045 (± 0.7)		1.044 (± 0.6)		
21	Female	41	Yes	1.036 (± 0.005)	1.047 (± 1.1)	1.047 (± 1.1)		1.047 (± 1.1)		1.044 (± 0.8)			1.046 (± 1.0)	1.047 (± 1.1)
22	Female	51	Yes	1.033 (± 0.004)	1.047 (± 1.4)	1.047 (± 1.4)		1.047 (± 1.3)		1.044 (± 0.1)		1.044 (± 1.0)		
23	Female	52	No	1.043 (± 0.005)	1.046 (± 0.3)	1.047 (± 0.4)			1.047 (± 0.4)	1.043 (± 0.0)			1.045 (± 0.2)	
24	Male	45	Yes	1.053 (± 0.014)	1.046 (± 0.6)		1.045 (± 0.7)	1.046 (± 0.6)		1.043 (± 1.0)		1.042 (± 1.0)		1.046 (± 0.6)
25	Male	51	Yes	1.044 (± 0.007)	1.046 (± 0.2)		1.045 (± 0.1)	1.046 (± 0.2)		1.042 (± 0.1)		1.042 (± 0.2)		1.046 (± 0.2)
26	Female	47	Yes	1.048 (± 0.006)	1.046 (± 0.2)	1.046 (± 0.2)		1.046 (± 0.3)		1.042 (± 0.6)		1.042 (± 0.6)	1.044 (± 0.4)	1.046 (± 0.2)
27	Female	82	Yes	1.026 (± 0.008)	1.046 (± 1.9)	1.046 (± 1.9)		1.046 (± 1.9)		1.042 (± 0.5)		1.042 (± 1.5)		
28	Female	47	Yes	1.041 (± 0.005)	1.045 (± 0.5)	1.046 (± 0.5)		1.045 (± 0.4)		1.041 (± 0.1)			1.044 (± 0.3)	
29	Male	64	Yes	1.051 (± 0.010)	1.045 (± 0.6)		1.044 (± 0.7)	1.045 (± 0.6)		1.041 (± 0.9)		1.041 (± 1.0)		1.045 (± 0.6)
30	Male	47	Yes	1.061 (± 0.008)	1.044 (± 1.5)		1.043 (± 1.6)	1.044 (± 1.6)			1.053 (± 0.7)			
31	Male	45	Yes	1.040 (± 0.005)	1.044 (± 0.4)		1.043 (± 0.3)	1.044 (± 0.4)			1.053 (± 1.3)			1.044 (± 0.4)
32	Female	45	Yes	1.039 (± 0.005)	1.044 (± 0.5)	1.046 (± 0.6)		1.044 (± 0.5)		1.040 (± 0.1)		1.040 (± 0.1)	1.042 (± 0.3)	
33	Male	29	Yes	1.068 (± 0.006)	1.043 (± 2.3)		1.042 (± 2.4)	1.043 (± 2.3)			1.053 (± 1.4)			1.043 (± 2.4)
34	Female	62	Yes	1.030 (± 0.005)	1.043 (± 1.2)	1.043 (± 1.2)		1.043 (± 1.2)		1.038 (± 0.8)		1.038 (± 0.7)		1.043 (± 1.2)

35	Female	59	No	1.049 (± 0.010)	1.042 (± 0.6)	1.043 (± 0.5)			1.043 (± 0.5)	1.038 (± 0.0)			1.040 (± 0.8)	
36	Female	48	No	1.052 (± 0.005)	1.042 (± 1.0)	1.043 (± 0.9)			1.043 (± 0.9)	1.037 (± 0.4)			1.040 (± 1.2)	
37	Male	66	Yes	1.029 (± 0.004)	1.042 (± 1.2)		1.041 (± 1.1)	1.042 (± 1.2)		1.037 (± 0.8)		1.037 (± 0.7)		
38	Male	66	Yes	1.039 (± 0.004)	1.042 (± 0.3)		1.041 (± 0.2)	1.042 (± 0.2)		1.037 (± 0.2)		1.037 (± 0.2)		
39	Female	45	Yes	1.060 (± 0.006)	1.041 (± 1.7)	1.042 (± 1.7)		1.041 (± 1.8)			1.051 (± 0.8)			
40	Male	53	Yes	1.030 (± 0.005)	1.040 (± 1.0)		1.039 (± 0.9)	1.040 (± 1.0)		1.035 (± 0.5)		1.035 (± 0.4)		1.040 (± 1.0)
41	Female	50	Yes	1.031 (± 0.014)	1.040 (± 0.8)	1.041 (± 0.9)		1.040 (± 0.8)		1.035 (± 0.3)		1.035 (± 0.3)	1.038 (± 0.6)	1.040 (± 0.8)
42	Female	47	No	1.045 (± 0.006)	1.040 (± 0.4)	1.041 (± 0.4)			1.041 (± 0.4)		1.050 (± 0.6)			1.040 (± 0.5)
43	Male	53	Yes	1.022 (± 0.005)	1.040 (± 1.8)		1.039 (± 1.7)	1.040 (± 1.8)		1.035 (± 0.3)			1.038 (± 1.6)	
44	Female	72	No	1.039 (± 0.003)	1.038 (± 0.1)	1.039 (± 0.0)			1.039 (± 0.0)		1.049 (± 1.0)			1.038 (± 0.1)
45	Female	78	Yes	1.039 (± 0.004)	1.038 (± 0.1)	1.038 (± 0.1)		1.038 (± 0.1)		1.032 (± 0.7)		1.032 (± 0.7)	1.035 (± 0.4)	
46	Female	44	Yes	1.039 (± 0.004)	1.038 (± 0.1)	1.038 (± 0.1)		1.038 (± 0.1)		1.032 (± 0.7)			1.035 (± 0.4)	

Table III: Collagen turnover rates and $F^{14}C$ values of the cohort, according to sex, rupture status, and risk factors.
Abbreviations: AHT indicates Arterial hypertension; SD, Standard deviation

Patients (n=20)		**Hemodynamic parameters**											
Intracranial aneurysms (n=20)		Average WSS [Pa]		Maximum WSS [Pa]		Average NWSS [Pa]		Maximum NWSS [Pa]		Average OSI		Average RRT	
		M ± SD		M ± SD		M ± SD		M ± SD		M ± SD		M ± SD	
Rupture status													
	Yes	5.22 ± 0.81	p=0.72	46.64 ± 10.21	p=0.44	0.48 ± 0.05	p=0.44	4.03 ± 0.39	p=0.49	0.009 ± 0.002	p=0.49	2.81 ± 0.54	p=0.49
	No	4.52 ± 0.92		38.53 ± 11.81		0.41 ± 0.06		3.26 ± 0.62		0.005 ± 0.001		2.77 ± 0.49	
Arterial hypertension													
	Yes	4.51 ± 0.67	p=0.97	38.94 ± 6.68	p=0.85	0.47 ± 0.07	p=0.85	3.77 ± 0.47	p=0.85	0.013 ± 0.004	p=0.01	2.83 ± 0.74	p=0.91
	No	5.35 ± 0.94		47.72 ± 12.48		0.45 ± 0.05		3.84 ± 0.47		0.004 ± 0.001		2.78 ± 0.47	
Current smoking													
	Yes	5.34 ± 1.08	p=1.0	48.56 ± 16.09	p=0.94	0.43 ± 0.05	p=0.71	3.78 ± 0.66	p=0.71	0.005 ± 0.001	p=0.08	2.61 ± 0.35	p=0.71
	No	4.74 ± 0.74		40.64 ± 6.37		0.48 ± 0.06		3.82 ± 0.30		0.010 ± 0.003		2.95 ± 0.68	
Aneurysm irregularity													
	Yes	4.67 ± 0.74	p=0.94	36.09 ± 4.56	p=0.77	0.50 ± 0.06	p=0.46	3.75 ± 0.31	p=1.0	0.012 ± 0.003	p=0.01	2.64 ± 0.67	p=0.46
	No	5.29 ± 0.98		50.84 ± 13.77		0.42 ± 0.05		3.84 ± 0.56		0.004 ± 0.001		2.93 ± 0.50	

Table IV: Hemodynamic parameters according to rupture status, and risk factors.

Abbreviations: WSS indicates Wall shear stress; Pa, Pascal; NWSS, Normalized wall shear stress; OSI, Oscillatory shear index; RRT, Relative residence time; M, Mean; SD, Standard deviation; P, Probability

Supplemental Figures

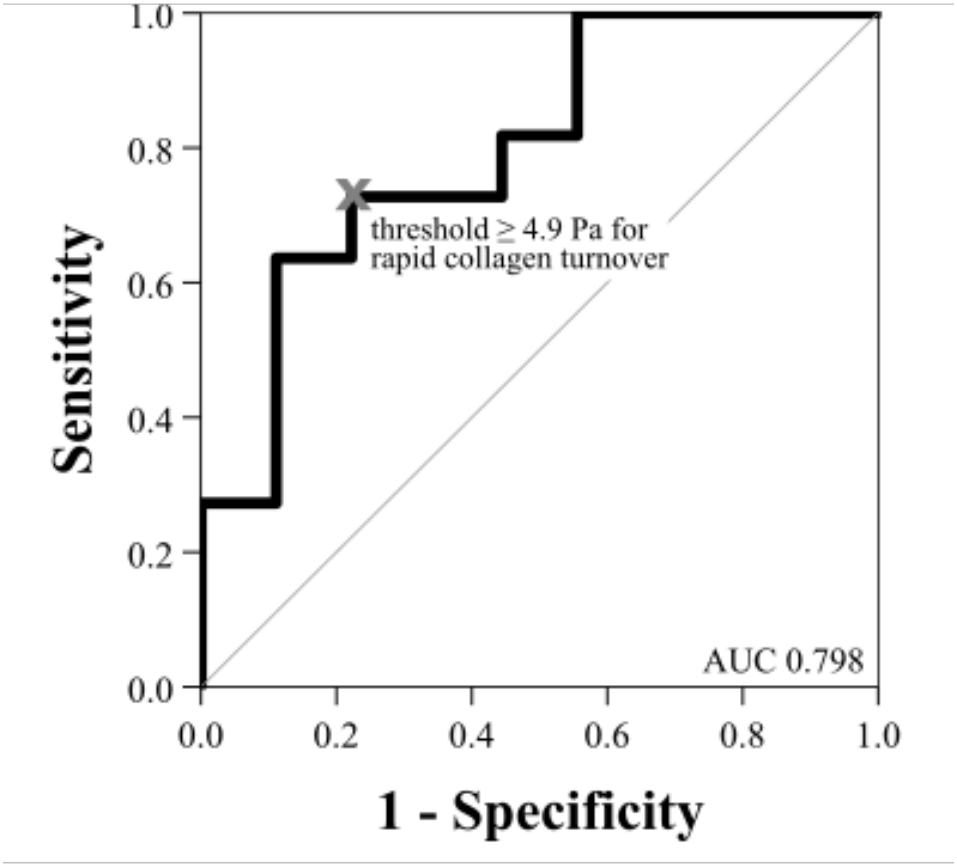

Figure I: Receiver operating characteristics-analysis of aneurysm time-averaged wall shear stress for differentiation between low and rapid collagen turnover (sensitivity 72.7 %, specificity 77.8 %).
Abbreviations: AUC indicates Area under the curve

Supplemental References

1. Etminan N, Dreier R, Buchholz BA, Beseoglu K, Bruckner P, Matzenauer C, et al. Age of collagen in intracranial saccular aneurysms. *Stroke*. 2014;45:1757-1763.
2. Bernard S, Frisen J, Spalding KL. A mathematical model for the interpretation of nuclear bomb test derived 14C incorporation in biological systems. Nuclear Instruments and Methods in Physics Research Section B: Beam Interactions with Materials and Atoms. 2010;268:1295-1298.
3. Spalding KL, Arner E, Westermark PO, Bernard S, Buchholz BA, Bergmann O, et al. Dynamics of fat cell turnover in humans. Nature. 2008;453:783-787.
4. Heinemeier KM, Schjerling P, Ohlenschlaeger TF, Eismark C, Olsen J, Kjaer M. Carbon-14 bomb pulse dating shows that tendinopathy is preceded by years of abnormally high collagen turnover. FASEB journal : official publication of the Federation of American Societies for Experimental Biology. 2018;32:4763-4775.
5. Antiga L, Piccinelli M, Botti L, Ene-Iordache B, Remuzzi A, Steinman DA. An image-based modeling framework for patient-specific computational hemodynamics. Medical & biological engineering & computing. 2008;46:1097-1112.
6. Xiang J, Yu J, Snyder KV, Levy EI, Siddiqui AH, Meng H. Hemodynamic-morphological discriminant models for intracranial aneurysm rupture remain stable with increasing sample size. Journal of neurointerventional surgery. 2016;8:104-110.
7. Murray CD. The Physiological Principle of Minimum Work: I. The Vascular System and the Cost of Blood Volume. Proceedings of the National Academy of Sciences of the United States of America. 1926;12:207-214.
8. Meng H, Tutino VM, Xiang J, Siddiqui A. High WSS or low WSS? Complex interactions of hemodynamics with intracranial aneurysm initiation, growth, and rupture: toward a unifying hypothesis. AJNR Am J Neuroradiol. 2014;35:1254-1262.
9. Adult Tobacco Use Information, Glossary. National Health Interview Survey. Centers for Disease Control and Prevention, National Center for Health Statistics. https://www.cdc.gov/nchs/nhis/tobacco/tobacco_glossary.htm. Accessed December 28, 2019.
10. Rittie L. Method for Picrosirius Red-Polarization Detection of Collagen Fibers in Tissue Sections. Methods in molecular biology. 2017;1627:395-407.
11. Sharma R, Rehani S, Mehendiratta M, Kardam P, Kumra M, Mathias Y, et al. Architectural Analysis of Picrosirius Red Stained Collagen in Oral Epithelial Dysplasia and Oral Squamous Cell Carcinoma using Polarization Microscopy. Journal of clinical and diagnostic research : JCDR. 2015;9:EC13-16.